# Influence of the aspect ratio and boundary conditions on universal finite-size scaling functions in the athermal metastable two-dimensional random field Ising model

Víctor Navas-Portella[1,2] and Eduard Vives[1]

[1]*Departament d'Estructura i Constituents de la Matèria, Facultat de Física, Universitat de Barcelona, Diagonal 645, 08028 Barcelona, Catalonia, Spain*

[2]*Centre de Recerca Matemàtica, Edifici C, Campus Bellaterra, E-08193 Bellaterra, Catalonia, Spain*

(Received 26 November 2015; revised manuscript received 15 January 2016; published 18 February 2016)

This work studies universal finite size scaling functions for the number of one-dimensional spanning avalanches in a two-dimensional (2D) disordered system with boundary conditions of different nature and different aspect ratios. To this end, we will consider the 2D random field Ising model at $T = 0$ driven by the external field $H$ with athermal dynamics implemented with periodic and forced boundary conditions. We have chosen a convenient scaling variable $z$ that accounts for the deformation of the distance to the critical point caused by the aspect ratio. In addition, assuming that the dependence of the finite size scaling functions on the aspect ratio can be accounted for by an additional multiplicative factor, we have been able to collapse data for different system sizes, different aspect ratios, and different types of the boundary conditions into a single scaling function $\hat{\mathcal{Q}}$.

DOI: 10.1103/PhysRevE.93.022129

## I. INTRODUCTION

The theory of universal finite-size scaling (FSS) functions has been broadly used in simulations of finite systems close to criticality in order to extrapolate numerical results to the thermodynamic limit [1]. In two-dimensional (2D) square lattices of sizes $L_x \times L_y$, these functions depend on the aspect ratio $a = L_y/L_x$ [2]. The properties of universal FSS functions when the aspect ratio, as well as boundary conditions, are changed have been studied in different works [3–10].

Within the context of percolation theory [11], analysis of the effects of rectangular boundaries on the spanning probability was studied by Langlands [3], who numerically showed that at the critical threshold there exists a universal scaling function of the aspect ratio. The study was based on symmetry arguments for the crossing probabilities. Inspired by the numerical results of Langlands, Cardy [4] derived an analytical expression using conformal invariance of the spanning probability in 2D percolation. Other numerical studies deal with both this problem as well as some variations in geometries and boundary conditions [5–7]. Okabe *et al.* studied shape effects and boundary conditions for Ising models [8,9] by analyzing the Binder parameter and magnetization curves. Hucht also studied symmetries of universal FSS functions in anisotropic systems by checking a symmetry hypothesis through Monte Carlo simulations of the 2D in-plane Ising model [10].

To the best of our knowledge, the effects of having a rectangular shape as well as different boundary conditions on FSS functions have not been studied in the 2D random field Ising model (RFIM) with athermal dynamics [12]. In this case, we would expect that quenched disorder as well as the metastable character of the dynamics would strongly determine the spanning cluster [11].

The athermal ($T = 0$) RFIM has been commonly used to explain Barkhausen noise in ferromagnetic materials [13]. In many cases, ferromagnetic coupling is so strong that it is not necessary to consider temperature as a relevant parameter in the model. During the field-driven magnetization process, free energy barriers are so large that thermally activated events are negligible. By considering interactions between spins, quenched disorder in the sample, and the external magnetic field, the RFIM offers a good explanation of hysteresis and crackling noise (avalanche dynamics).

The model is also applicable to other physical systems such as structural transitions, capillary condensation of gases in porous solids, etc. [13,14]. All of these phenomena commonly share the existence of a first-order phase transition and hysteresis. Metastable states separated by high-energy barriers appear in the free energy landscape.

When the external force is increased (for example, the magnetic field), the conjugated variable (magnetization) responds discontinuously. These nonequilibrium collective events, known as "avalanches," are essentially due to the system jumping from one metastable state to another. The properties of these avalanches strongly depend on the quenched disorder present in the system, which determines which sites of the system are more favorable to nucleate or not.

The lower critical dimension of the RFIM is known to be $d_c = 2$ in the equilibrium case [15]. This implies that ferromagnetic order will not occur for $d \leqslant 2$. It is not completely clear if the lower critical dimension is still $d_c = 2$ for the RFIM with local metastable dynamics at $T = 0$. Sethna and coworkers opened the door to a possible existence of long-range order in this case [16]. Nevertheless, it has been necessary to examine larger system sizes in order to determine whether the critical value of the model parameter determining the amount of quenched disorder $\sigma_c$ was finite or not, in the thermodynamic limit. Recently Spasojević and coworkers found numerical evidence of a critical point, below which ($\sigma < \sigma_c$) the system orders ferromagnetically. This evidence was based on the FSS collapse of the curves corresponding to magnetization [17], distribution of avalanche sizes [18], and number of spanning avalanches [19].

In order to study the effect of both the aspect ratio and boundary conditions on universal FSS functions, we will focus on the number of spanning avalanches in one direction [19,20]. Spanning avalanches, strictly speaking, are well-defined objects only in finite-size simulations with square or rectangular boundaries. They correspond to magnetization events of size $S$ that extend, at least, from one side of the system to the

 

opposite one. They can be classified as one-dimensional (1D) spanning or 2D spanning, depending on whether they span the system in one or two spatial directions. Nevertheless, in the thermodynamic limit such avalanches correspond to infinite objects not necessarily massive (i.e., $S/L^2 \to 0$) similar to the infinite cluster [11] within percolation theory.

Different strategies may help in understanding the critical nature of such objects. A first possibility is to study their behavior when the shape of the finite system is changed by simulating not only square, but also rectangular, boundary conditions with a certain aspect ratio $a$. A second strategy is to study spanning objects when the physical nature of the finite boundaries is changed. Numerical simulations often use periodic boundary conditions (PBCs). Such spatial boundaries are the most adequate to minimize finite-size effects when studying a first-order phase transition that occurs due to a local nucleation process. However, some forced boundary conditions may help in the understanding of models with propagating front dynamics. Typically, this is done by keeping periodic boundaries in one direction, while fixing the boundaries in the other direction to be in the two different coexisting phases. We will refer to these as fixed boundary conditions (FBCs). Seppälä *et al.* [21] found evidence of front roughening effects in the equilibrium RFIM at $T = 0$ with FBCs without an external field. The model has metastable dynamics but is restricted to nucleation close to the interface. This model was studied within the context of a depinning transition [22] and was also used for the study of morphological changes in the invading front [23]. The ground state of the equilibrium three-dimensional (3D) RFIM was studied by Middleton and Fisher by using a variety of fixed boundary conditions, and then the results were compared with periodic boundaries [24].

In this work, we present a numerical study of the number of 1D spanning avalanches $N_1$ in the metastable 2D RFIM using the two strategies described above. The subscript 1 is not relevant for this paper but will be kept in order to be consistent with previous works [19,20]. The model and the simulation details are presented in Sec. II. Results corresponding to the FSS analysis for rectangular PBCs are presented in Sec. III A. We will obtain FSS functions that include the dependence on the aspect ratio $a$. The analysis of FBCs and different aspect ratios is presented in Sec. III B. In this case we obtain FSS functions with two additive contributions: the first is the same as for PBCs, and the second one is related to a roughening transition of the interface. Finally, a summary and conclusions are presented in Sec. IV.

## II. MODEL

Ising models consist of an ensemble of $N$ interactive spins situated at the nodes of a $D$-dimensional lattice. Spins can take the values $s_i = \pm 1$. The RFIM is a variant of these kinds of models, which includes quenched disorder (impurities, dislocations, vacancies, etc.), that distorts the free-energy landscape. The Hamiltonian describing this model is

$$\mathcal{H} = -\sum_{\langle ij \rangle} J s_i s_j - \sum_i (H + h_i) s_i. \tag{1}$$

The first term accounts for the ferromagnetic interaction with nearest neighbors. For simplicity, we consider $J = 1$. $H$ is the external field and $\{h_i\}$ are local quenched random fields, which are independent and Gaussian distributed according to

$$\rho(h) = \frac{1}{\sqrt{2\pi\sigma^2}} \exp\left(-\frac{h^2}{2\sigma^2}\right), \tag{2}$$

where $\sigma$ characterizes the amount of disorder present in the system. We study a 2D square lattice with a rectangular shape ($N = L_x \times L_y, a = L_y/L_x$). In order to generate metastable dynamics, it is necessary to establish a criterion to determine under which conditions the system remains at a local minimum of the energy landscape. Following Sethna's rule [12], a spin is stable when it is aligned with its effective field:

$$h_i^{\text{eff}} = \sum_k^z s_k + H + h_i, \tag{3}$$

where the sum extends over the $z$ neighbors of the spin $s_i$, which in the case of a 2D square lattice is $z = 4$. Following this deterministic rule, a spin flips when its effective field changes sign. A flipping event changes the value $h_k^{\text{eff}}$ of its nearest neighbors, and any of these could become unstable. The process continues in the same way analyzing successive shells and originating an avalanche of flipping spins. The size $S$ of the avalanche corresponds to the number of spins that have changed their state, whereas the duration $T$ corresponds to the number of shells needed to complete the avalanche. Simulations start with all the spins pointing downwards ($\{s_i = -1\}$) and $H = -\infty$. The external field is increased until a spin triggers an avalanche. The external field is then kept constant until there are no more unstable spins and the system reaches a metastable state again. The dynamical process finishes when all the spins are pointing up ($\{s_i = +1\}$) for a very large positive value of the field $H$. The Sorted List algorithm has been implemented [25]. Since our intention is not to discuss the behavior in the thermodynamic limit but to understand FSS relations, it has been preferable to study characteristic sizes of $L_x, L_y \leqslant 1024$ and perform a number of averages over many ($10^5$) realizations of the random fields. The results presented in this work are valid for aspect ratios ranging from $a = 1/2$ to $a = 2$. For illustrative purposes we will also show numerical results for smaller values of $a$ ($a = 1/4$ and $a = 1/8$).

## III. RESULTS

### A. Periodic boundary conditions (PBCs)

The field-driven, athermal RFIM with the standard PBCs and $L_x = L_y \equiv L$ has been broadly studied [16–19]. By numerical analysis it is shown that there exists a continuous transition for a finite value of disorder $\sigma_c = 0.54$ which separates two different regimes [16,17]. For $\sigma < \sigma_c$, there is an infinite avalanche, which is usually 2D spanning [see Figs. 1(a)–1(c), which correspond to increasing field values]. When disorder approaches its critical value $\sigma_c$, there is a peak in the average number of 1D spanning avalanches [19] [see Figs. 1(d)–1(f)]. Power-law distributions are found for some magnitudes related to avalanches for this model (sizes and durations). For the regime $\sigma > \sigma_c$, the magnetization process takes place by nucleation of small domains that grow and

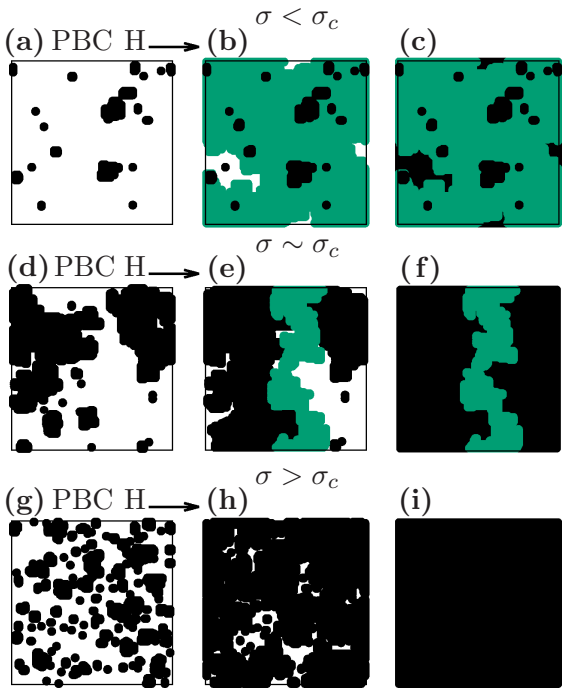


FIG. 1. Sequence of configurations during the magnetization process in different disorder regimes for the RFIM with metastable dynamics for a system ($L = 128$) with PBCs. The values of the disorder are $\sigma = 0.80, 0.95, 1.20$ for sequences (a–c), (d–f), and (g–i), respectively. The external field $H$ is increased from left to right bringing the system from negative magnetization (white regions) to positive magnetization (colored regions). Black colored spins correspond to regions that have been transformed due to nonspanning avalanches. Green regions correspond to spanning avalanches.

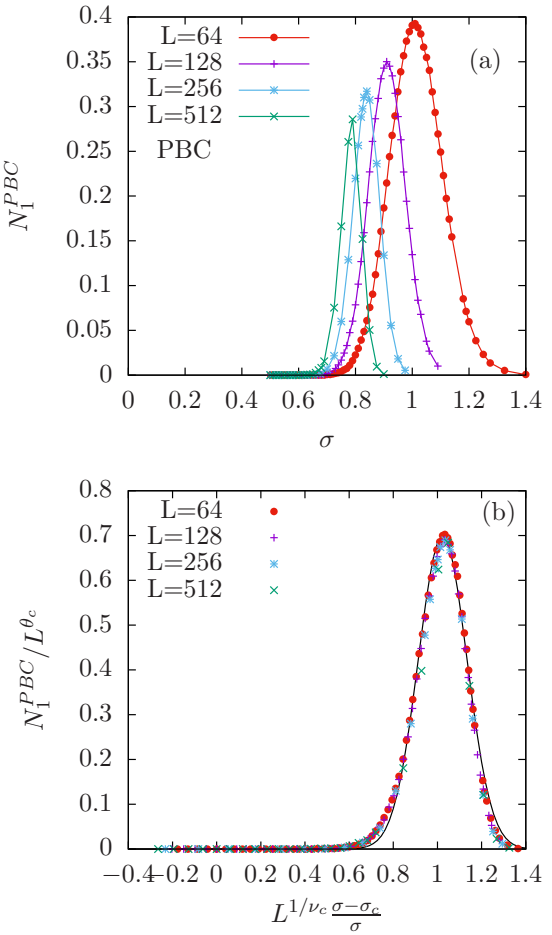


FIG. 2. (a) Average number of 1D spanning avalanches per magnetization process versus the disorder $\sigma$ for different sizes in a square systems $a = 1$ with PBCs. Lines are guides to the eye. (b) Curve collapse for different system sizes by using Eq. (4). The solid black line represents a Gaussian fit of the scaled data.

coalesce, and there is no presence of spanning avalanches [see Figs. 1(g)–1(i)]. The average number of 1D spanning avalanches during the full magnetization process from $H = -\infty$ to $H = +\infty$ as a function of the disorder $\sigma$ is presented in Fig. 2 for square systems ($L_x = L_y = L; a = 1$).

In Fig. 2(a), the number of 1D spanning avalanches exhibits a peak at the value of disorder $\sigma_c(L)$ as found by Spasojević *et al.* [19]. These peaks present the following scaling behavior:

$$N_1^{PBC}(\sigma, L) = L^{\theta_c}\mathcal{P}\left(L^{1/\nu_c}\frac{\sigma-\sigma_c}{\sigma}\right), \tag{4}$$

where $\sigma_c = 0.54 \pm 0.03$, $\frac{1}{\nu_c} = 0.19 \pm 0.02$, $\theta_c = -0.10 \pm 0.03$, and $\mathcal{P}$ is the FSS function related to the number of 1D spanning avalanches for PBCs [see Fig. 2(b)]. These values are compatible with those of Ref. [19].The error bars of the fitted parameters account for variations that still offer acceptable collapses. We use the calligraphic letter $\mathcal{P}$ for the scaling functions with PBCs. Note that in this case, as opposed to what happens in the 3D case [20], the number of 1D spanning avalanches vanishes in the thermodynamic limit due to the negative sign of the exponent $\theta_c$.

In the present work, we will study rectangular PBCs, and thus we have to separate spanning avalanches in the $\hat{y}$ and $\hat{x}$ direction. Therefore, we will measure $N_1^{y;PBC}(\sigma, L_x, a)$, $N_1^{x;PBC}(\sigma, L_x, a)$, where we have chosen a dependence on the disorder $\sigma$, the horizontal width $L_x$ and the aspect ratio $a = L_y/L_x$. In order to perform the FSS analysis we need to find a scaling variable for this rectangular case. The geometric average length $L = \sqrt{L_x L_y}$ is used in Ref. [7] for FSS of asymmetric systems of percolating sticks. We have checked that, with this choice of the scaling length, it is not possible to achieve collapses for different aspect ratios. We propose an alternative choice of the scaling length that enables curves to collapse both for different sizes as well as for different aspect ratios $a$. Due to asymmetry ($a \neq 1$), there is an easy direction for the system to percolate, which is $\min(L_x, L_y)$. In an infinite system, the correlation length at the critical point will diverge symmetrically in the $\hat{x}$ and $\hat{y}$ directions as

$$\xi \sim \left(\frac{\sigma-\sigma_c}{\sigma}\right)^{-\nu}. \tag{5}$$

Note that we measure the distance to the critical point $\sigma_c$ with the same function as in Ref. [19], instead of the standard choice $(\sigma - \sigma_c)/\sigma_c$. This issue was already proposed in the previous works on the RFIM [12] and was extensively discussed in Ref. [20]. The direction for easy percolation is the one which first limits a 1D spanning avalanche. Thus, in the limits of

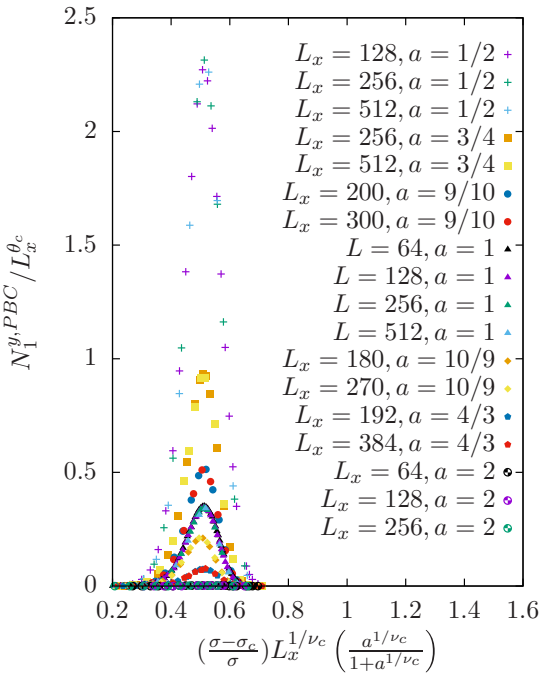


FIG. 3. Curve collapses $\mathcal{P}_a^y(z)$ for the number of 1D spanning avalanches in the $\hat{y}$ direction with the same aspect ratio $a$ and different sizes.

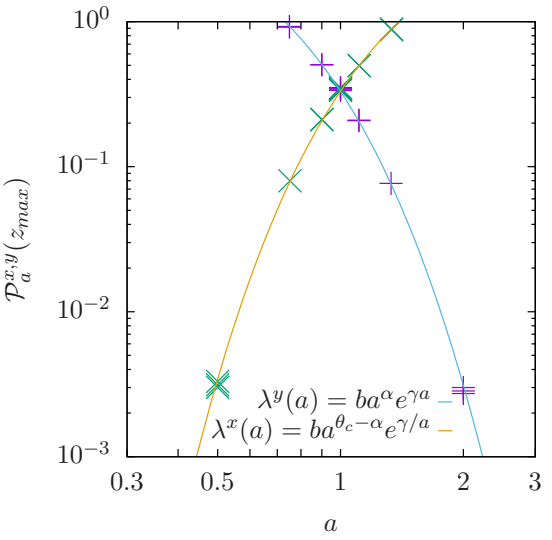


FIG. 4. Log-log plot of the peak heights $\mathcal{P}_a^{x,y}(z_{\max})$ as a function of the aspect ratio $a$ and fits of functions $\lambda^x(a)$ and $\lambda^y(a)$ as described in the text.

$a \ll 1$ and $a \gg 1$, a finite system will experience pseudo-critical effects when the correlation length approaches

$$\xi \sim L = \min(L_x, L_y). \tag{6}$$

The function $\min(L_x, L_y)$ exhibits a discontinuous derivative at $a = 1$. In order to avoid it, we propose measuring the limit of the correlation length as

$$L = L_x \frac{a}{(1 + a^{1/\nu_c})^{\nu_c}}, \tag{7}$$

and the corresponding scaling variable

$$z = L_x^{1/\nu_c}\left(\frac{a^{1/\nu_c}}{1 + a^{1/\nu_c}}\right)\frac{\sigma - \sigma_c}{\sigma}. \tag{8}$$

Note that this choice results in $z = \min(L_x, L_y)^{1/\nu_c}((\sigma - \sigma_c)/\sigma)$ for the limits $a \ll 1$ and $a \gg 1$. As shown in Fig. 3, curve collapses for 1D spanning avalanches in the $\hat{x}$ or $\hat{y}$ direction are achieved independently for each aspect ratio. Furthermore, the peaks are aligned on the same abscissa:

$$N_1^{x,PBC}(\sigma, L_x, a) = L_x^{\theta_c}\mathcal{P}_a^x(z), \tag{9}$$

$$N_1^{y,PBC}(\sigma, L_x, a) = L_x^{\theta_c}\mathcal{P}_a^y(z), \tag{10}$$

with the same parameters $\theta_c$, $\nu_c$, and $\sigma_c$ as in Eq. (4). Strictly speaking, we show only data for $N_1^{y,PBC}$, but one must take into account the fact that the number of 1D spanning avalanches satisfies the following symmetry:

$$N_1^{y,PBC}(\sigma, L_x, a) = N_1^{x,PBC}\left(\sigma, aL_x, \frac{1}{a}\right). \tag{11}$$

A similar expression was proposed in Ref. [3] for the spanning probability in percolation theory. If one applies this symmetry to Eq. (10), the following relation between FSS functions must be fulfilled:

$$\mathcal{P}_a^x(z) = a^{\theta_c}\mathcal{P}_{1/a}^y(z). \tag{12}$$

In order to assert the dependence of the scaling functions on the aspect ratio $a$, we propose that these functions $\mathcal{P}_a^x(z)$ and

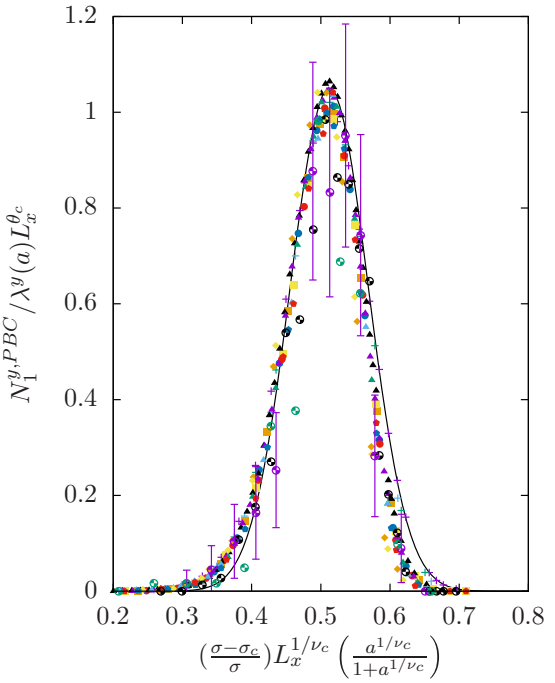


FIG. 5. Curve collapses for 1D spanning avalanches in the $\hat{y}$ direction for different aspect ratios and sizes. Same point and color code as in Fig. 3. The black solid line corresponds to the Gaussian fit of Fig. 2(b). Example of typical error bars corresponding to $a = 2$ is shown.

$\mathcal{P}_a^y(z)$ can be written in the following way:

$$\mathcal{P}_a^x(z) = \lambda^x(a)\hat{\mathcal{P}}^x(z), \tag{13}$$

$$\mathcal{P}_a^y(z) = \lambda^y(a)\hat{\mathcal{P}}^y(z), \tag{14}$$

where $\lambda^x(a)$, $\lambda^y(a)$ are functions of the parameter $a$. Note that the functions $\lambda^x(a)$ and $\lambda^y(a)$ are different if one considers 1D spanning avalanches in the $\hat{x}$ or $\hat{y}$ direction. From the study of the peak heights $\mathcal{P}_a^{x,y}(z_{\max})$ a good fit (see Fig. 4) can be obtained with

$$\lambda^x(a) = ba^{\theta_c-\alpha}e^{\gamma/a}, \tag{15}$$

$$\lambda^y(a) = ba^{\alpha}e^{\gamma a}, \tag{16}$$

where $b = 80 \pm 42$, $\alpha = 1.2 \pm 0.4$, and $\gamma = -5.5 \pm 0.5$. One must take into account the fact that $b, \alpha$ and $\gamma$ have an empirical character and play no role in the following developments. Note that this choice satisfies the following symmetry requirement:

$$\frac{\lambda^x(a)}{\lambda^y(1/a)} = a^{\theta_c}. \tag{17}$$

From this last equality and Eqs. (13) and (14) one obtains

$$\hat{\mathcal{P}}^x(z) = \hat{\mathcal{P}}^y(z) \equiv \hat{\mathcal{P}}(z), \tag{18}$$

which means that, in fact, we can formulate a scaling function $\hat{\mathcal{P}}$ independent of the spatial direction. Taking into account all these premises, satisfactory collapses of the whole set of numerical data are obtained with the following FSS hypothesis:

$$N_1^x(\sigma, L_x, a) = L_x^{\theta_c}\lambda^x(a)\hat{\mathcal{P}}(z), \tag{19}$$

$$N_1^y(\sigma, L_x, a) = L_x^{\theta_c}\lambda^y(a)\hat{\mathcal{P}}(z). \tag{20}$$

Overlaps for peaks corresponding to $N_1^{y,PBC}$ are shown in Fig. 5.

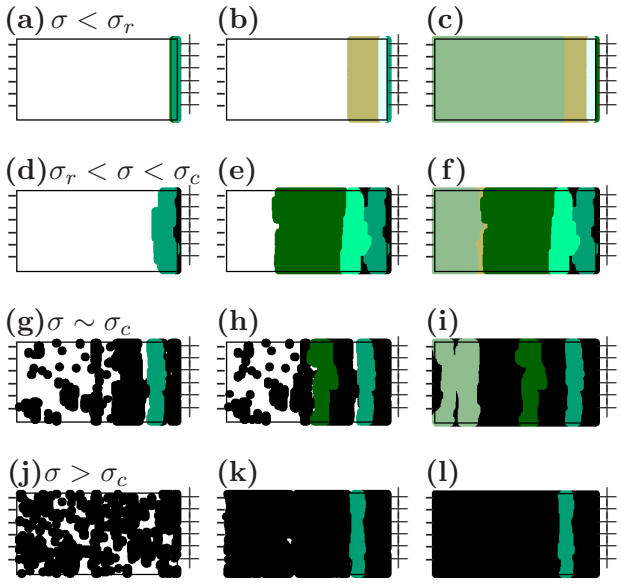


FIG. 6. Sequence of configurations during the magnetization process for the field-driven, athermal RFIM with metastable dynamics under FBCs for a system with $L_x = 512$ and aspect ratio $a = 1/8$. The values of the disorder are $\sigma = 0.25, 0.50, 0.90, 1.20$ for sequences (a–c), (d–f), (g–i), and (j–l), respectively. The external field $H$ increases from left to right. Symbols (+) and (−) correspond to spins which have values $s_i = +1$ and $s_i = -1$, respectively, and conform the fixed boundaries. Black colored regions correspond to nonspanning avalanches, whereas 1D spanning avalanches are represented by different shades of green. A front that advances from right to left is easily identified in sequences (a–c), (d–f), and (g–i).

### B. Fixed boundary conditions (FBCs)

The idea behind imposing FBCs is to force simulations to exhibit a domain wall which can be identified as an advancing front (see Fig. 6). From a physical point of view, this would represent a situation in which the system under study is a subset of a larger one with an already formed interface. By keeping periodic boundaries in the vertical $\hat{y}$ direction, the horizontal $\hat{x}$ direction is subjected to the following condition: at the boundary $x = L_x + 1$, there is a column of spins $\{s_i = +1\}$

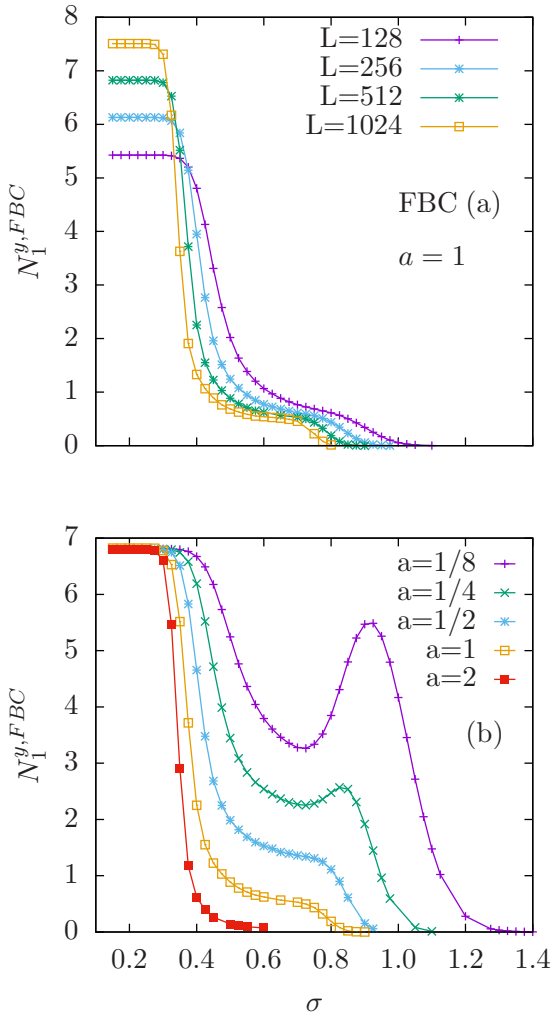


FIG. 7. (a) Average number of 1D spanning avalanches in the $\hat{y}$ direction as a function of the disorder for a system with $a = 1$ and different sizes. (b) Average number of 1D spanning avalanches in the $\hat{y}$ direction as a function of disorder for different aspect ratios for a system with $L_x = 512$. Lines are guides to the eye.

(+ symbols in Fig. 6), while at $x = 0$ there is a column of spins $\{s_i = -1\}$ (− symbols in Fig. 6). Under these specific conditions, 1D spanning avalanches in the $\hat{y}$ direction are more common in a regime of low disorder. A minuscule fraction of 1D spanning avalanches are found in the $\hat{x}$ direction, while 2D spanning avalanches have no relevant statistical weight.

When the system presents a stripe geometry ($a < 1$), it is easy to distinguish four different regimes for the dynamics of 1D spanning avalanches as a function of the disorder $\sigma$. Below a certain value of the quenched disorder, $\sigma < \sigma_r$, a sequence of massive spanning avalanches with a flat interface appears during the magnetization process [see Figs. 6(a)–6(c)]. As disorder increases, there exists a regime ($\sigma_r < \sigma < \sigma_c$) where the advancing front presents a rough profile and there is a negligible presence of nucleated domains in front of the advancing interface [Figs. 6(d)–6(f)]. When disorder approaches its critical value ($\sigma \sim \sigma_c$), the critical interface advances interacting with many nucleated domains [Figs. 6(g)–6(i)]. Above $\sigma_c$, it is unlikely to find a 1D spanning avalanche so the front is ill-defined except for some very rare cases [Figs. 6(j)–6(l)]. For higher disorders, a pure nucleation and growth process is recovered.

The main goal of this section is to study the consequence of changing the nature of the boundaries on the FSS functions and to relate them with those found with PBCs for any aspect ratio $a$ in the regime dominated by critical effects.

As can be observed in Fig. 7(a), two steps are clearly distinguished in the behavior of the number of 1D spanning avalanches $N_1^{y,FBC}(\sigma)$. The higher step on the left is related to the morphological transition of the propagating front. This transition separates the regimes where there is a sequence of 1D spanning avalanches with a flat profile (faceted growth) and the regime where 1D spanning avalanches exhibit a certain rough profile. The second step occurs in the region $\sigma \sim 0.8$

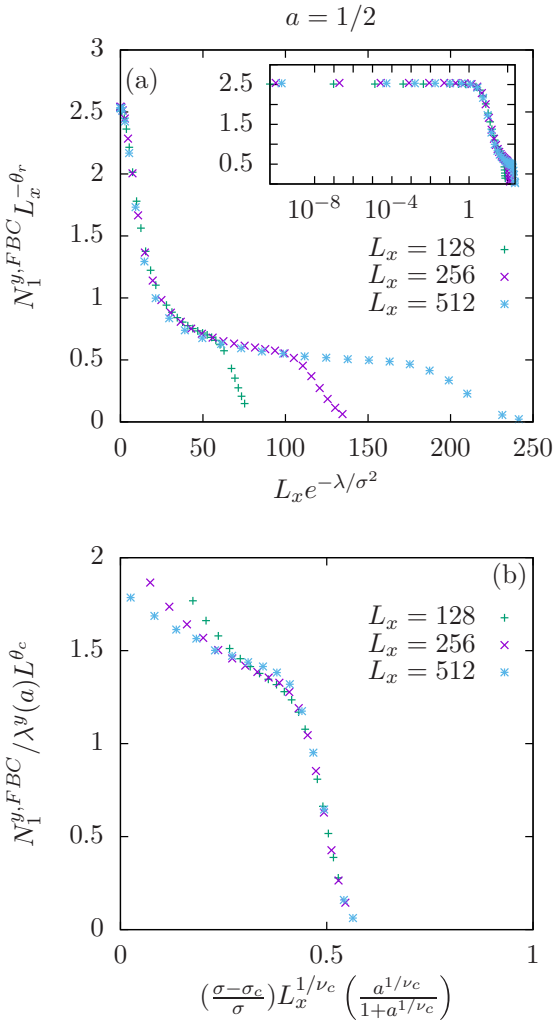


FIG. 8. Curve collapse for average number of 1D spanning avalanches per magnetization process for different system sizes in a system with $a = 1/2$. (a) Partial curve collapse in the regime dominated by roughening. The step can be appreciated in the inset plot where the same figure is represented using a logarithmic scale on the horizontal axis. (b) The partial curve collapse for the regime dominated by the bulk critical transition.

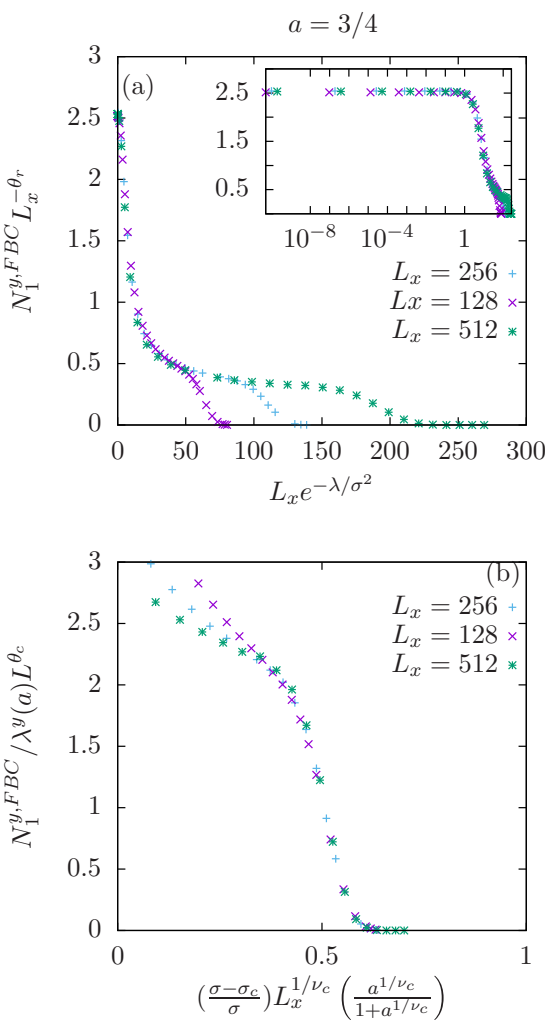


FIG. 9. Curve collapse for average number of 1D spanning avalanches per magnetization process for different system sizes in a system with $a = 3/4$. (a) The partial curve collapse in the regime dominated by roughening. The step can be appreciated in the inset plot where the same figure is represented with a logarithmic scale on the horizontal axis. (b) The partial curve collapse for the regime dominated by the critical transition.

where, in the case of PBCs, the peaks are found. This suggests that the steps are related to the critical transition.

Note that at low disorder the average number of spanning avalanches $N_1^{y,FBC}$ reaches values above five, whereas for similar system sizes and disorder $N_1^{PBC}$ with PBCs is negligible [see Fig. 2(a)]. A qualitative argument to justify such a difference is given as follows: in the low disorder regime, local fields take values around zero. As spins near the boundary $x = L_x$ have a neighbor which is pointing upwards $\{s_i = +1\}$ the external field needs to be around $H = 2$ in order to flip it and create a nucleation center for a 1D spanning avalanche that propagates in the $\hat{y}$ direction. In the model with PBCs, the external field needs to be around $H = 4$ in order to flip a spin and generate a nucleation center which can span the system in one or two directions. When the system is subjected to FBCs, it is very difficult to find a horizontal spanning avalanche which connects both sides of the system with fixed boundaries as well as 2D spanning avalanches.

In order to elucidate how the height of the observed steps depends on system size and shape, simulations at different $L_x$ and $L_y$ have been performed. Results for fixed $L_x$ and different aspect ratios are shown in Fig. 7(b). Note that the height of the step on the left does not depend on $a$. This indicates that the horizontal length $L_x$ controls the number of 1D spanning avalanches at low disorders. By changing the aspect ratio, the morphology of the curves in Fig. 7(b) changes. When $a$ is lower than unity, which means that the system is dominated by periodic boundaries, critical effects are strengthened and what seemed to be a step for $a = 1$ becomes a clear peak. As the aspect ratio increases, the sides of the system which are subjected to fixed boundaries take over and critical effects are gradually hindered. This suggests that, in the critical region, invariance under 90-degree rotations is recovered for disorders close to $\sigma_c$ and the same analysis as in the previous section can be performed.

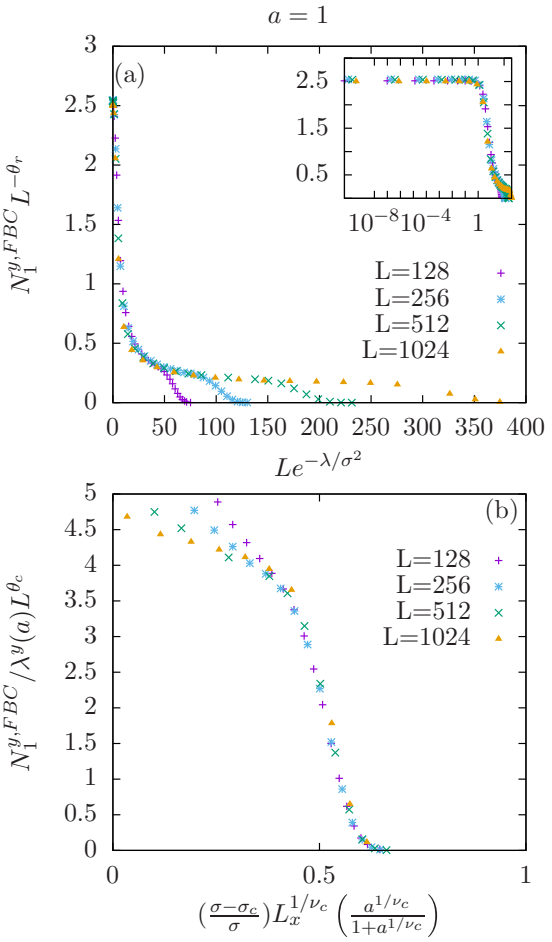


FIG. 10. Curve collapse for average number of 1D spanning avalanches per magnetization process for different system sizes in a square system $L_x = L_y \equiv L$. (a) Partial curve collapse in the regime dominated by roughening effects. The step can be appreciated in the inset plot where the same figure is represented with a logarithmic scale on the horizontal axis. (b) Partial curve collapse for the regime dominated by the critical transition.

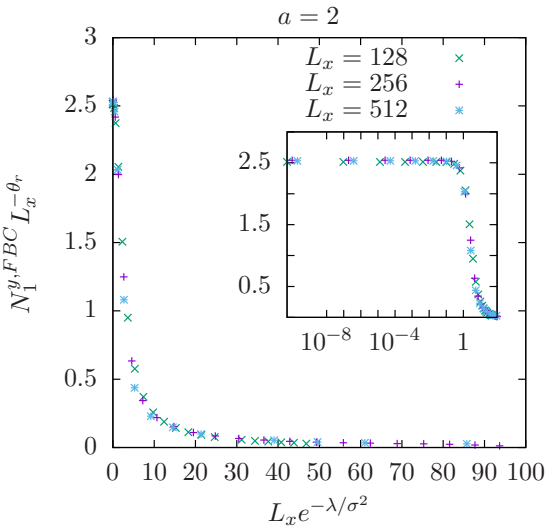


FIG. 11. Curve collapse for average number of 1D spanning avalanches per magnetization process for different system sizes in a system with $a = 2$. The step can be appreciated in the inset plot, where the same figure is represented with a logarithmic scale on the horizontal axis. In this case, critical effects have been hindered and the contribution of spanning avalanches in the critical region is negligible.

The discussion above suggests that we should propose a combined FSS relation with parameters related to both transitions $(\sigma_c,\sigma_r)$ in order to achieve a partial curve collapse. For a certain aspect ratio, the scaling hypothesis is

$$N_1^y(\sigma, L_x, aL_x) = L_x^{\theta_r}\hat{\tilde{\mathcal{F}}}_a(\tilde{z}) + L_x^{\theta_c}\lambda^y(a)\hat{\mathcal{F}}(z), \qquad (21)$$

where $\tilde{z} = L_x e^{-\lambda/\sigma^2}$ is the scaling variable in the roughening regime with $\lambda = 0.64 \pm 0.03$ and $\theta_r = 0.16 \pm 0.01$. This choice of the scaling variable $\tilde{z}$ had already been proposed in Refs. [16] and [26]. It means that the roughening transition occurs for a certain value of the disorder only due to finite-size effects. Faceted growth will not be present in the thermodynamic limit for Gaussian random fields, as also explained by Ji and Robbins [23]. We will use the calligraphic letter $\mathcal{F}$ for the FSS functions corresponding to FBCs. Partial collapses in the roughening regime are shown in Fig. 8(a) for $a = 1/2$, Fig. 9(a) for $a = 3/4$, Fig. 10(a) for $a = 1$, and Fig. 11 for $a = 2$. Curves clearly overlap when the scaling

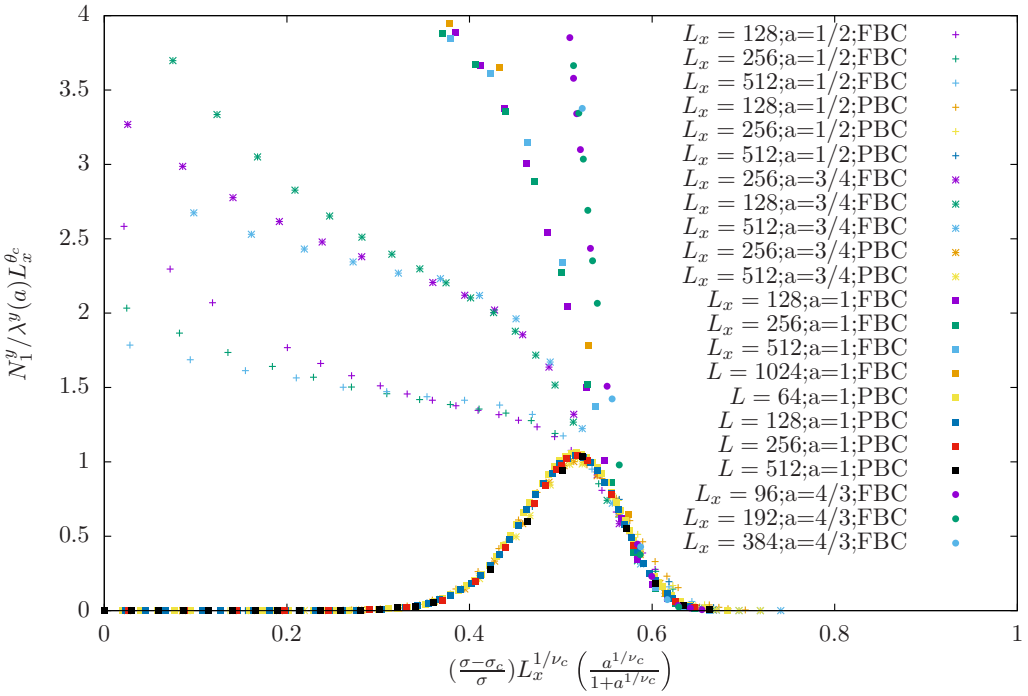


FIG. 12. Overlaps of FSS functions with FBCs and PBCs. Equation (22) is satisfied for $a = \{1/2,3/4,1,4/3\}$.

variable is below 50 approximately. The second term of Eq. (21) has the same form and the same scaling variable as in Eq. (20) from the previous section. Partial curve collapses in the critical region are shown in Fig. 8(b) for $a = 1/2$, in Fig. 9(b) for $a = 3/4$ and in Fig. 10(b) for $a = 1$. Note that the hypothesis of combined FSS remains valid for different aspect ratios, where the critical effects have a greater presence (Fig. 8) or have practically disappeared (Fig. 11).

Finally, let us test the relation between FSS functions for PBCs and FBCs in the critical region. Figure 12 shows that indeed, both FSS functions are equivalent:

$$\hat{\mathcal{P}}(z) = \hat{\mathcal{F}}(z) \equiv \hat{\mathcal{Q}}(z). \tag{22}$$

Note that we achieve partial overlaps of data corresponding to FBCs and PBCs corresponding to $a = \{1/2,3/4, 1, 4/3\}$. Consequently, the FSS function $\hat{\mathcal{Q}}(z)$ does not depend on $a$ or on the nature of the boundary conditions. Note that the smaller (larger) the aspect ratio, the broader (smaller) the range of agreement between FSS functions. This makes sense since, as explained in Fig. 7(b), for aspect ratios greater than unity critical effects are hindered. The left-hand tails of peaks found for PBCs cannot be related to the curves for FBCs. In this regime and for the studied system sizes the presence of the FBCs is still too strong to appreciate critical effects.

## IV. SUMMARY AND CONCLUSIONS

In this work we have presented results corresponding to the field-driven, athermal RFIM with local relaxation dynamics with PBCs and FBCs and rectangular geometries with different aspect ratios $a$. We have proposed a new scaling variable

$$z = L_x^{1/\nu_c}\left(\frac{a^{1/\nu_c}}{1+a^{1/\nu_c}}\right)\frac{\sigma-\sigma_c}{\sigma}. \tag{23}$$

With this choice, the average number of 1D spanning avalanches in $\hat{x}$ and $\hat{y}$ directions can be scaled as

$$N_1^{x,y}(\sigma,L_x,a) = L_x^{\theta_c}\lambda^{x,y}(a)\tilde{\mathcal{Q}}(z), \tag{24}$$

where the functions $\lambda^{x,y}$ depend on whether we study 1D spanning avalanches in the $\hat{x}$ or $\hat{y}$ direction and satisfy

$$\frac{\lambda^x(a)}{\lambda^y(1/a)} = a^{\theta_c}. \tag{25}$$

The physical meaning of these prefactors $\lambda^{x,y}$ accounts for the relative increase or decrease of the number of 1D spanning avalanches when the aspect ratio is changed. With these definitions, the scaling function $\hat{\mathcal{Q}}$ is thus independent of the aspect ratio $a$ and, even more, independent of the nature of the boundary conditions. To observe the collapses corresponding to Eq. (20) for the case of FBCs, it is only possible for large enough values of $z$ so that the effects caused by the faceted growth of the interfaces become irrelevant.

In future works it would be interesting (a) to perform the same study for the 3D case and (b) to study the morphological properties of the advancing front and its dynamics for different amounts of disorder.

## ACKNOWLEDGMENTS

This work was completed with computational resources provided by IBERGRID collaboration. Financial support was received from Ministerio de Economía y Competitividad (Spain) (Project No. MAT2015-69777-REDT and Project No. MAT2013-40590-P) and from Fundació la Caixa. We would like to thank the referee for suggesting the scaling variable in Eq. (8), which improved our previous choice. We also acknowledge D. Spasojević for fruitful discussions during a visit to the Universitat de Barcelona.

[1] V. Privman, in *Finite Size Scaling and Numerical Simulations of Statistical Systems*, edited by V. Privman (World Scientific, Singapore, 1990), Chap. 1.

[2] K. Binder, in *Finite Size Scaling and Numerical Simulations of Statistical Systems*, edited by V. Privman (World Scientific, Singapore, 1990), Chap. 4.

[3] R. P. Langlands, C. Pichet, Ph. Pouliot, and Y. Saint-Aubin, On the universality of crossing probabilities in two-dimensional percolation, J. Stat. Phys. **67**, 553 (1992).

[4] J. L. Cardy, Critical percolation in finite geometries, J. Phys. A **25**, L201 (1992).

[5] M. Masihi, P. R King, and P. Nurafza, Effect of anisotropy on finite-size scaling in percolation theory, Phys. Rev. E **74**, 042102 (2006).

[6] H. Watanabe, S. Yukawa, N. Ito, and C.-K. Hu, Superscaling of Percolation on Rectangular Domains, Phys. Rev. Lett. **93**, 190601 (2004).

[7] M. Zezelj, I. Stankovic, and A. Belic, Finite size scaling in asymmetric systems of percolating sticks, Phys. Rev. E **85**, 021101 (2012).

[8] Y. Okabe, K. Kaneda, M. Kikuchi, and C. K. Hu, Universal finite size scaling functions for critical systems with tilted boundary conditions, Phys. Rev. E **59**, 1585 (1999).

[9] K. Kaneda, Y. Okabe, and M. Kikuchi, Shape effects of finite size scaling functions for anisotropic three-dimensional Ising models, Phys. A: Math. Gen. **32**, 7263 (1999).

[10] A. Hucht, On the symmetry of universal finite-size scaling functions in anisotropic systems, J. Phys. A: Math. Gen. **35**, L481 (2002).

[11] D. Stauffer and A. Aharony, *Introduction to Percolation Theory*, 2nd ed. (Taylor and Francis, London, 1994).

[12] J. P. Sethna, K. Dahmen, S. Kartha, J. A. Krumhansl, B. W. Roberts, and J. D. Shore, Hysteresis and Hierarchies: Dynamics of Disorder-Driven First-Order Phase Transitions, Phys. Rev. Lett. **70**, 3347 (1993).

[13] J. P. Sethna, K. A. Dahmen, and O. Perkovic, in *The Science of Hysteresis*, edited by G. Bertotti and I. Mayergoyz, Vol. 2 (Academic Press, Amsterdam, 2006), pp. 105–179.

[14] M. L. Rosinberg and E. Vives, Recent topics on metastability, hysteresis, avalanches, and acoustic emission associated to martensitic transitions in functional materials, in *Disorder and Strain-Induced Complexity in Functional Materials*, edited by T. Kakeshita, T. Fukuda, A. Saxena, and A. Planes, Springer Series in Materials Science, Vol. 148 (Springer Heidelberg, 2012).

[15] M. Aizenman and J. Wehr, Rounding of First-Order Phase Transitions in Systems With Quenched Disorder, Phys. Rev. Lett. **62**, 2503 (1989).

[16] O. Perkovic, K. A. Dahmen, and J. P. Sethna, Disorder-induced critical phenomena in hysteresis: A numerical scaling analysis, arXiv:cond-mat/9609072 (1996).

[17] D. Spasojević, S. Janićević, and M. Knezević, Numerical Evidence for Critical Behavior of the Two-Dimensional Nonequilibrium Zero-Temperature Random Field Ising Model, Phys. Rev. Lett. **106**, 175701 (2011).

[18] D. Spasojević, Sanja Janićević, and Milan Knezević, Avalanche distributions in the two-dimensional nonequilibrium zero-temperature random field Ising model, Phys. Rev. E **84**, 051119 (2011).

[19] D. Spasojević, Sanja Janićević, and Milan Knezević, Analysis of spanning avalanches in the two-dimensional nonequilibrium zero-temperature random-field Ising model, Phys. Rev. E **89**, 012118 (2014).

[20] F. J. Pérez-Reche and E. Vives, Spanning avalanches in the three-dimensional Gaussian random-field Ising model with metastable dynamics: Field dependence and geometrical properties, Phys. Rev. B **70**, 214422 (2004).

[21] E. T Seppälä, V. Petäjä, and M. J. Alava, Disorder, order, and domain wall roughening in the 2D random field Ising model, Phys. Rev. E **58**, R5217 (1998).

[22] B. Drossel and K. Dahmen, Depinning of a domain wall in the 2d random-field Ising model, Eur. Phys. J. B **3**, 485 (1998).

[23] H. Ji and M. O. Robbins, Transition from compact to self-similar growth in disordered systems: Fluid invasion and magnetic-domain growth, Phys. Rev. A **44**, 2538 (1991).

[24] A. A. Middleton and D. S. Fisher, Three-dimensional random-field Ising magnet: Interfaces, scaling, and the nature of states, Phys. Rev. B **65**, 134411 (2002).

[25] M. C. Kuntz, O. Perković, K. A. Dahmen, B. W. Roberts, and J. P. Sethna, Hysteresis, Avalanches, and Noise, Comput. Sci. Eng. **1**, 73 (1999).

[26] A. J. Bray and M. A. Moore, Scaling theory of the random-field Ising model, J. Phys. C **18**, L927 (1985).